Effects of Diabatic Cooling in a Shear Flow with a Critical Level

YUH-LANG LIN AND HYE-YEONG CHUN

Department of Marine, Earth, and Atmospheric Sciences, North Carolina State University, Raleigh, North Carolina

(Manuscript received 9 July 1990, in final form 12 February 1991)

ABSTRACT

The response of a two-dimensional, stably stratified shear flow to diabatic cooling, which represents the evaporative cooling of falling precipitation in the subcloud layer, is examined using both a linear analytical theory and a nonlinear numerical model. The ambient wind is allowed to reverse its direction at a certain height and the cooling is specified from the surface to a height below the wind reversal level.

From a scale analysis of the governing equations, a nonlinearity factor of the thermally induced finite-amplitude wave, $gQ_0l/(c_pT_0U_0^2N)$, is found. From a scale analysis of the linear system, it is shown that the wind shear can modify the condition in which the upstream propagation of the density current is opposed by the ambient wind. When the shear and the basic wind are of opposite sign, small basic wind is enough to prevent the upstream propagation of the density current. This is because part of the cooling is used to compensate the positive vorticity associated with the positive wind shear. Therefore, the effective cooling rate, or the speed of the density current, becomes smaller than that in the uniform wind case.

In the nonlinear numerical simulations, it is found that the response of the atmosphere to a steady cooling in a shear flow may be categorized as either a *stationary cold pool* or a *density current*, depending upon the strength of the effective cooling. For a strong shear flow, the cold pool is stationary with respect to the upstream flow because most of the cooling is used to compensate the positive vorticity associated with the positive wind shear. In this case, the response is similar to the linear steady-state case. For a weak shear flow, the cold pool is able to propagate upstream because the effective cooling, which increases with time, is strong enough to push the outflow against the basic wind. From the comparison of linear and nonlinear numerical model simulations, it is found that the nonlinearity appears to reduce the wave disturbance below the critical height and above the cooling top, while it tends to strengthen the density current or cold pool near the surface.

1. Introduction

The cold air outflow produced by the evaporation of falling precipitation in the subcloud layer has been regarded as one of the important mechanisms for convective storm dynamics. Many observational and numerical studies have indicated that the cold air outflow from thunderstorms can trigger and maintain convective storms (e.g., Charba 1974; Mitchell and Hovermale 1977; Matthews 1981; Thorpe et al. 1982; Seitter 1986; Droegemeier and Wilhelmson 1987). The leading edge of the outflow, called a gust front, tends to lift air parcels ahead of it and generate deep convection under favorable conditions.

Environmental wind shear is a crucial dynamic factor that can either enhance or suppress deep convection. Vertical wind shear has long been observed as an important factor in the convective storm dynamics (Newton 1950; Newton and Newton 1959; Pastushkov 1975; Ogura and Liou 1980). Effects of vertical wind shear and rain-produced cold pools on the maintenance and generation of long-lived convective systems have been a main research topic in the numerical modeling studies (e.g., Thorpe et al. 1982; Weisman and Klemp 1982; Rotunno et al. 1988; Weisman et al. 1988; Fovell and Ogura 1989). Thorpe et al. (1982) proposed that a strong low-level wind shear can prevent outflow from moving away from convective cells, thus, providing a favorable condition for long-lived convective systems. Rotunno et al. (1988) suggested that when the cold pool is balanced by the wind shear, the circulation induced by a cold pool trying to spread downshear is opposed by the wind shear and a deep penetration may take place. Fovell and Ogura (1989) showed that in multicellular storms wind shear is linearly proportional to the density current speed for a large value of wind shear. In studies pursuing the dynamical similarlity between a laboratory-produced density current and a thunderstorm outflow, the vertical shear of the basic flow has been ignored. Recently, Droegemeier and Wilhelmson (1985a,b) investigated the effects of vertical wind shear on convective cloud formation using a three-dimensional numerical model. They found that the vertical wind shear controls characteristics of the cloud forming along an outflow collision line.

In theoretical studies, the evaporative cooling in the subcloud layer associated with the thunderstorm

Corresponding author address: Dr. Yuh-Lang Lin, Dept. of Marine, Earth, and Atmospheric Sciences, North Carolina State University, Box 8208, Raleigh, NC 27695-8208.

downdraft is often specified by a local heat sink. Thorpe et al. (1980) investigated the dynamics of the downdraft using a two-dimensional steady-state analytical model and a nonlinear numerical model with a specified cooling. Several authors (e.g., Smith and Lin 1982; Lin and Smith 1986; Raymond 1986) have studied linear responses of a stratified atmosphere to a local heat source or sink in a uniform environmental flow. These theoretical studies pointed out that the response of the atmosphere to a specified heating or cooling can be characterized by a thermally induced Froude number, U/Nd, where d is the heating or cooling depth. This dependency of the flow response on the Froude number was also explained in terms of group velocity by Bretherton (1988). Recently, Raymond and Rotunno (1989) studied the response of a stratified fluid to a specified cooling in a uniform flow using a nonlinear numerical model. They found that the flow can be characterized by two nondimensional parameters that combine three types of speed: basic wind speed, horizontal speed of the dominant gravity wave, and upstream propagation speed of the density current. They concluded that in a stably stratified boundary layer, the response of the atmosphere to cooling resembles gravity waves rather than a density current, except when the cooling is strong enough to produce faster outflow speed than gravity waves. As mentioned above, the vertical wind shear may play an important role in the initiation and/or maintenance of mesoscale convective systems. Therefore, it is important to extend these types of studies to include the vertical wind shear.

It is often observed in midlatitude squall lines that a level exists at which the basic wind normal to the line is equal to the propagation speed of the moving system. This level is often referred to as the critical level. Observations by Ogura and Liou (1980) indicate that a typical midlatitude squall line exhibits a critical level near 6 km. Climatological studies by Bluestein and Jain (1985) and Wyss and Emanuel (1988) also have shown that most midlatitude squall lines have a critical level near 6 km. In the simulation of midlatitude squall lines using a wave–CISK model, Raymond (1984) used a linear shear with a critical level for the downshear mode. The linear response of a stably stratified atmosphere to a local heating in a constant shear flow with a critical level has been investigated by Lin (1987) and Lin and Li (1988). They found that the low-level vertical velocity is strongly dependent upon the vertical wind shear and heating depth. In a linear theory, Booker and Bretherton (1967) found that when an internal gravity wave approaches a critical level, most of the wave energy is absorbed there and only a small amount of wave energy can be transmitted if the Richardson number of the basic flow is larger than one-fourth. Using a nonlinear model, Breeding (1972) showed that for a relatively small Richardson number a considerable amount of the incident wave is reflected, while for a large Richardson number, the response is similar to that in a linear case. If the incident wave is in phase with the reflected wave, wave resonance is possible in the lower layer. It remains unclear how the cooling-induced nonlinear wave behaves if a critical level exists. In addition, one should examine whether there are any waves being reflected from the top boundary of the model.

The purpose of this study is to investigate the effects of diabatic cooling in a two-dimensional shear flow with a critical level using both a linear analytical theory and a nonlinear numerical model. In section 2, the governing equations are presented and the nonlinearity parameter of thermally induced finite-amplitude waves is discussed. In section 3, linear steady-state solutions and a condition for which the density current is able to propagate upstream against the wind shear are obtained. The numerical model description and results with different wind shears are discussed in section 4. In addition, nonlinear effects of a critical level are compared with the wave-breaking theory in a corresponding mountain-wave problem. Summary and conclusions are presented in the last section.

2. Governing equations

The governing equations of a two-dimensional, hydrostatic, Boussinesq, nonrotating flow can be written as

$$u_t + (U + u)u_x + wu_z + U_z w + \pi_x = 0, \quad (1)$$

$$\pi_z = b, \quad (2)$$

$$b_t + (U + u)b_x + wb_z + N^2 w = gQ/(c_p T_0), \quad (3)$$

$$u_x + w_z = 0, \quad (4)$$

where u and w are the perturbation horizontal and vertical wind velocities, π is the kinematic pressure perturbation (p/ρ_0), b the buoyancy perturbation, U the horizontal basic wind, N the Brunt–Väisälä frequency, g the gravitational acceleration, c_p the specific heat capacity at constant pressure, and T_0 a constant reference temperature. The Q represents diabatic cooling, which is assumed to have a form of $Q(x, z) = Q_0 f(x) h(z)$, where Q_0 is the amplitude of the cooling rate and $f(x)$ and $h(z)$ are the distribution functions of the cooling in the horizontal and vertical. In this study, N is assumed to be constant and U is given by

$$U(z) = -U_0 + \alpha z, \quad (5)$$

where α $(\equiv U_0/H_c)$ is the constant wind shear. Here U_0 is the magnitude of the basic flow at the surface and H_c is the wind reversal height. Equations (1)–(4) can be combined into two prognostic equations of vorticity and buoyancy,

$$\varphi_{zzt} + U\varphi_{zzx} + b_x - J(\varphi, \varphi_{zz}) = 0, \quad (6)$$

$$b_t + Ub_x - N^2\varphi_x - J(\varphi, b) = gQ/(c_p T_0), \quad (7)$$

where φ is the streamfunction defined by $\varphi_x = -w$, $\varphi_z = u$. Notice that φ_{zz} is the vorticity under the hydrostatic approximation. The symbol J represents the Jacobian defined by $J(A, B) = A_x B_z - A_z B_x$. We may introduce the following nondimensional variables:

$$\tilde{t} = (U_0/l)t, \quad \tilde{x} = x/l, \quad \tilde{z} = (N/U_0)z,$$
$$\tilde{U} = U/U_0, \quad \tilde{\varphi} = [c_p T_0 N^2/(gQ_0 l)]\varphi,$$
$$\tilde{b} = [c_p T_0 U_0/(gQ_0 l)]b, \quad \tilde{Q} = \tilde{f}(x)\tilde{h}(z),$$
$$\tilde{H}_c = NH_c/U,$$

where l is the horizontal length of the cooling. After nondimensionalization, Eqs. (6) and (7) become (the tildes are dropped in the rest of this section and section 3)

$$\varphi_{zzt} + U\varphi_{zzx} + b_x - \mu J(\varphi, \varphi_{zz}) = 0, \tag{8}$$

$$b_t + Ub_x - \varphi_x - \mu J(\varphi, b) = Q, \tag{9}$$

where μ is defined by

$$\mu = gQ_0 l/(c_p T_0 U_0^2 N). \tag{10}$$

The μ represents the nonlinearity of thermally induced waves. In fact, μ can be interpreted as a scale ratio of the horizontal velocity perturbation to the basic wind. Equation (10) indicates that the amplitude of the wave is proportional to the cooling rate and the horizontal cooling length, and inversely proportional to the square of the surface wind speed and the Brunt–Väisälä frequency. Many theoretical and numerical studies have investigated nonlinearity factors in mountain-wave problems (Clark and Peltier 1977; Klemp and Lilly 1978; Peltier and Clark 1979; Barcilon 1985). However, no similar studies have been made for finite-amplitude waves induced by thermal forcing. For mountain waves with a mountain height of h, U_0/Nh (Froude number) has been proposed as a control parameter for wave amplitude. Smith and Lin (1982) showed that the amplitude of thermally induced waves, relative to the mountain waves, is determined by a nondimensional parameter $gQ_0 l/(c_p T_0 U_0^2 Nh)$ for a linear system with uniform flow. Notice that Q_0 has a different unit in Smith and Lin because the heating is concentrated at a certain level instead of distributed in a layer. They found that for a typical mountain height and heating rate, the amplitude of thermally induced waves may exceed that of orographically induced waves.

3. Linear analytical solutions

Under the assumptions of steady-state and small-amplitude perturbations, Eqs. (8) and (9) can be reduced to a single equation in φ (all variables are nondimensionalized):

$$U^2\varphi_{zzx} + \varphi_x = -Q. \tag{11}$$

After making the one-sided Fourier transform in x ($\rightarrow k$), the above equation becomes

$$U^2\hat{\varphi}_{zz} + \hat{\varphi} = i\hat{Q}/k. \tag{12}$$

The homogeneous part of the above equation is the Taylor–Goldstein equation. The solutions with a diabatic heating have been obtained by Lin (1987). Lin's solution has also been used as the initial condition for simulations of moist convection by Crook and Moncrieff (1988). The diabatic cooling, which represents the evaporative cooling of falling precipitation, is assumed to have the form

$$Q(x, z) = \begin{cases} a_1^2/(a_2^2 + x^2) - a_1 a_2/(a_2^2 + x^2), \\ \qquad\qquad \text{for} \quad 0 \leqslant z < d \\ 0, \quad \text{for} \quad z \geqslant d, \end{cases} \tag{13}$$

where a_1 and d denote the half-width of the bell-shaped function and the cooling depth, respectively. The cooling depth (d) is assumed to be smaller than the wind reversal height (H_c). The second term with a_2 in Eq. (13) is necessary to avoid the net cooling in an inviscid steady-state problem (Smith and Lin 1982; Bretherton 1988). Here, we have nondimensionalized a_1, a_2, and x by l. The structures of the cooling and the basic wind are sketched in Fig. 1. The cooling is concentrated in the shaded region. Making the Fourier transform of Eq. (13) and substituting it into Eq. (12) yields

$$U^2\hat{\varphi}_{zz} + \hat{\varphi} = \begin{cases} -a_1(e^{-a_1 k} - e^{-a_2 k}), \quad \text{for} \quad 0 \leqslant z < d \\ 0, \quad \text{for} \quad z \geqslant d. \end{cases} \tag{14}$$

Notice that the nondimensional form of Eq. (5) is $U(z) = -1 + z/H_c$. The wavenumber k is always positive since we have used a one-sided Fourier transform. Following the procedure of Lin (1987), we obtain the solution,

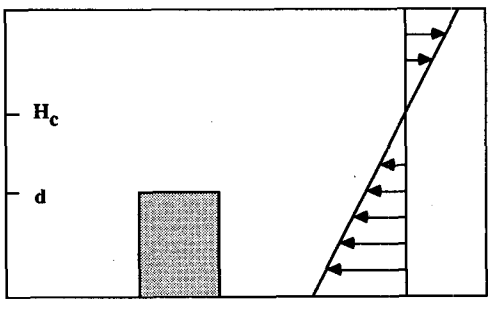

FIG. 1. Structures of basic horizontal wind and diabatic cooling used in this study. The symbols d and H_c represent the cooling depth and the wind reversal height, respectively. The cooling is concentrated in the shaded region.

$$\varphi(x, z) = [s_1\{\text{cosX1} - \text{cosX2} + s_2(\text{sinX1} - \text{sinX2})\} - s_3\,\text{cosX3}]\text{TNXI} - [s_1\{\text{sinX1} - \text{sinX2} - s_2(\text{cosX1} - \text{cosX2})\} - s_3\,\text{sinX3}]\text{LNXI} + \text{TNXI}, \quad \text{for} \quad 0 \leqslant z < d \quad (15a)$$

$$\varphi(x, z) = [s_1\{\text{cosX1} + \text{cosX2} + s_2(\text{sinX1} + \text{sinX2})\} - s_3\,\text{cosX3}]\text{TNXI} - [s_1\{\text{sinX1} - \text{sinX2} - s_2(\text{cosX1} - \text{cosX2})\} - s_3\,\text{sinX3}]\text{LNXI}, \quad \text{for} \quad d \leqslant z < H_c \quad (15b)$$

$$\varphi(x, z) = e^{-\pi\nu}[s_1\{s_2(\text{cosX1} - \text{cosX2}) - \text{sinX1} + \text{sinX2}\} + s_3\,\text{sinX3}]\text{TNXI} - e^{-\pi\nu}[s_1\{\text{cosX1} + \text{cosX2} + s_2(\text{sinX1} + \text{sinX2})\} - s_3\,\text{cosX3}]\text{LNXI}, \quad \text{for} \quad z \geqslant H_c \quad (15c)$$

where

$$\nu = (\text{Ri} - 1/4)^{1/2},$$

$$s_1 = 0.5\{|\text{Ri}^{1/2} - z|/(\text{Ri}^{1/2} - d)\}^{1/2},$$

$$s_2 = 0.5/\nu,$$

$$s_3 = \{|\text{Ri}^{1/2} - z|/\text{Ri}^{1/2}\}^{1/2},$$

$$\text{X1} = \nu \ln[\{(\text{Ri}^{1/2} - d)|\text{Ri}^{1/2} - z|\}/\text{Ri}],$$

$$\text{X2} = \nu \ln\{(\text{Ri}^{1/2} - d)/|\text{Ri}^{1/2} - z|\},$$

$$\text{X3} = \nu \ln\{|\text{Ri}^{1/2} - z|/\text{Ri}^{1/2}\},$$

$$\text{TNXI} = a_1[\tan^{-1}(x/a_2) - \tan^{-1}(x/a_1)],$$

$$\text{LNXI} = a_1[0.5 \ln\{(a_2^2 + x^2)/(a_1^2 + x^2)\}].$$

The linear assumption near the critical level breaks down because the vertical wavelength becomes infinitely small as the wave approaches the critical level and the horizontal perturbation velocity approaches infinity (Booker and Bretherton 1967). However, the above solutions are still valid outside the critical layer. In this study, we assume that the critical level is located above the cooling top and the Richardson number is greater than 1/4. When the wave propagates upward toward the critical level, most of the wave energy is absorbed there and attenuated by a factor of $e^{-\pi\nu}$. When the Richardson number is less than 1/4, the critical layer may act as a reflector. In the nonlinear regime, the wave behavior is different from that of the linear system. Breeding (1962) showed that for a relatively small Richardson number (<2.0), the critical layer can reflect a large amount of energy in the nonlinear flow even though the Richardson number is larger than 1/4. Breeding also found that the nonlinear response for a large Richardson number is similar to a linear one. However, the work of Breeding should be treated with caution since it had low resolution, and may be affected by reflections from the model boundaries. In addition, it used a periodic forcing rather than a steady-state forcing in the present study. We will investigate these effects in next section.

From Eq. (15), it can be seen that the wave amplitude is proportional to the reciprocal of $(\text{Ri}^{1/2} - d)^{1/2}$ or $\text{Ri}^{1/2}$. For a fixed cooling depth, the perturbation streamfunction is inversely proportional to the Richardson number. Thus, solution does not imply that the response is linearly proportional to the Richardson number as shown by Lin (1987). The difference comes from the different scale factors used in nondimensionalizing the governing equations. The Richardson number and the nondimensional diabatic heating term in Lin were defined by $\text{Ri} = (NH_c/U_0)^2$ and $Q = (Q_0 g l H_c)/(c_p T_0 U_0^3)$. Figure 2a shows the maximum perturbation streamfunction for different Richardson numbers and cooling depths in the domain calculated by Eq. (15) with $a_1 = 1$ and $a_2 = 5$. The magnitude is independent of the Richardson number for a small cooling depth, while it increases as the Richardson number decreases for a large cooling depth. Figure 2b shows the maximum vertical-velocity field in the domain for the same range of Richardson numbers and cooling depths. As shown in Fig. 2b, the vertical velocity is independent of the Richardson number for small cooling depth, while the magnitude is strongly dependent on the Richardson number for large cooling depth and strong shear. However, a maximum value exists near Ri = 4.0 and $d = 1.67$. Notice that near Ri = 3.0 and $d = 1.7$, the linear solution breaks down because $(\text{Ri}^{1/2} - d)$ is almost zero, and s_1, X1, and X2 in Eq. (15) approach infinity.

Figure 3 shows the total streamfunction and vertical-velocity fields with $N = 0.01\ \text{s}^{-1}$, $U_0 = 20\ \text{m s}^{-1}$, $Q_0 = -1\ \text{J kg}^{-1}\ \text{s}^{-1}$, $d = 2.0$ km, $a_1 = 10$ km, $a_2 = 50$ km, and $H_c = 2.5$ km. The Richardson number associated with the basic flow is 1.56. The streamfunction, vertical velocity, and other parameters shown in Fig. 3 are in dimensional values. Below the wind reversal level, a strong updraft is located at the upstream edge of the cooling region and a weaker downdraft at the downstream edge. The updraft at the upstream edge is associated with the compensated downdraft, which moves downstream (Lin and Smith 1986). The downshear tilt of the downdraft below the critical level is caused by the advection effect of the basic wind as shown by Lin (1987). Above the critical level, almost no perturbations are found because the waves are attenuated exponentially as they pass through the critical level (Booker and Bretherton 1967). Figure 4 shows the maximum vertical velocity for different wind shears with the same parameters used for Fig. 3. Since the critical height is fixed, large surface wind speed implies strong wind shear and small Richardson number. When the surface wind is larger than 15 m s^{-1} or is between 5 and 7.5 m s^{-1}, the maximum vertical ve-

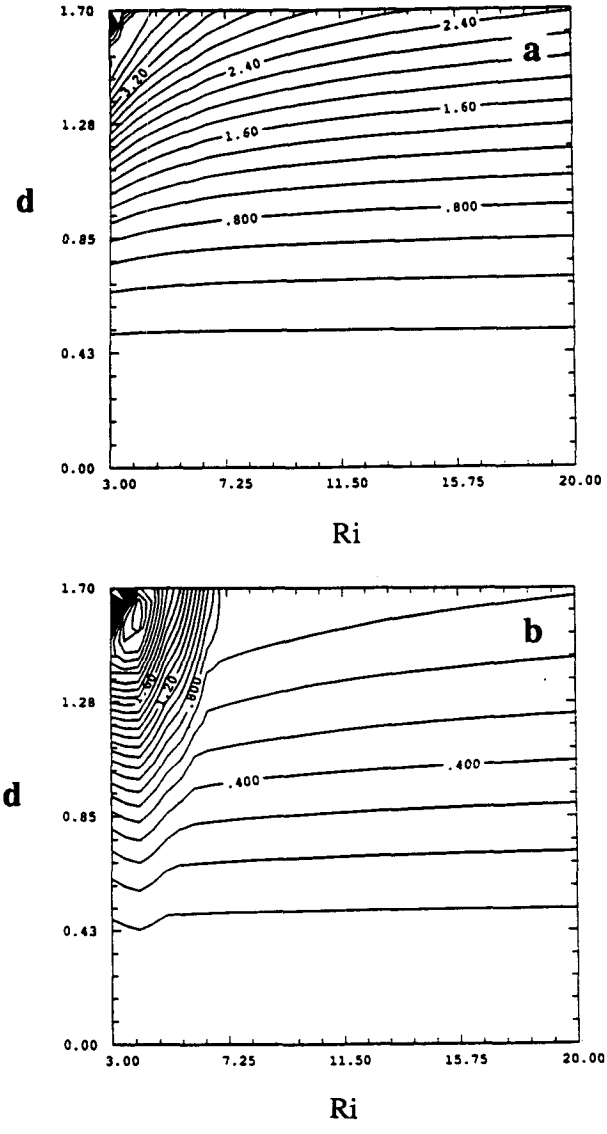

FIG. 2. (a) The domain maximum perturbation streamfunction for different cooling depths and the Richardson numbers from Eq. (15). (b) As in (a) except for the maximum vertical velocity. All variables are nondimensionalized.

locity decreases as the wind shear increases. The response is opposite otherwise. Notice that the linear solution is not valid for the surface wind speed below or near 5 m s^{-1} because the nonlinear effect becomes important and cannot be ignored. These three different characteristics of the solutions may be related to the combinations of three types of speed, as suggested by Raymond and Rotunno (1989). For the given parameters, the speed of the density current and the horizontal speed of gravity waves with a vertical wavelength of 2d, defined by $[Q_0gld/(c_pT_0)]^{1/3}$ and (Nd/π), are 10.91 m s^{-1} and 6.36 m s^{-1}, respectively. The surface wind that can prevent upstream propagation of the density current is approximately greater than or equal to 15 m s^{-1} when the ambient wind is taken as the averaged basic wind in the cooling layer. Also, the gravity wave is able to propagate upstream when the surface wind is smaller than 7.5 m s^{-1} because the averaged ambient wind speed against the upstream propagation of the gravity wave is smaller than the horizontal speed of the gravity wave in this case. Raymond and Rotunno (1989) found a condition in which the upstream density current is just opposed by the ambient wind.

For a flow with constant shear, we find the following relationships:

$$u^*/|U| = \frac{[Q_0gld/(c_pT_0)]/|U|^3}{1 - U_zd/U + d^2N^2/U^2}, \quad (16)$$

$$F = F_c = F_0\left[\frac{G^2}{(1 - \beta_0U_zd/U)G^2 + G_0^2}\right]^{1/3}, \quad (17)$$

where u^* is the perturbation horizontal velocity in the cooling region and F_0, G_0, and β_0 are proportionally constants. We define F and G by

$$F = |U|/[Q_0gld/(c_pT_0)]^{1/3}, \; G = \pi|U|/(Nd). \quad (18)$$

Equations (16) and (17) are similar to Eqs. (10) and (11) of Raymond and Rotunno (1989) for a uniform flow case. In a shear flow, $|U|$ can vary with the cooling depth and F and G are functions of height. Equations (16) and (17) indicate that the wind shear modifies the relative magnitude of density current speed and basic wind speed, which can prevent upstream propagation of the density current. The effect of wind shear is determined by the sign of U_zd/U. For a positive wind shear in the flow coming from right to left, U_zd/U becomes negative and the denominator of Eq. (16) becomes larger than that in the uniform flow case. This implies that smaller ambient wind is enough to prevent an upstream-propagating density current for a positive wind shear. This is because part of the cooling is used to compensate the positive vorticity generated by the positive vertical wind shear. Accordingly, the effective cooling rate, or the speed of the density current, becomes smaller than that for the uniform flow case. Thorpe et al. (1982) showed that a relatively large value of inflow speed is necessary to prevent the upstream propagation of a density current for a uniform flow and suggested that the vertical wind shear may modify that value. From Eqs. (16) and (17), it is clear that the vertical wind shear at the lower layer makes the upstream-propagating density current more stationary, which is important for initiation and regeneration of deep convections.

4. Nonlinear numerical simulations

a. Model description

In this section, we develop a time-dependent, nonlinear numerical model based on Eqs. (1)–(4) with subgrid-scale mixing included. The hydrostatic ap-

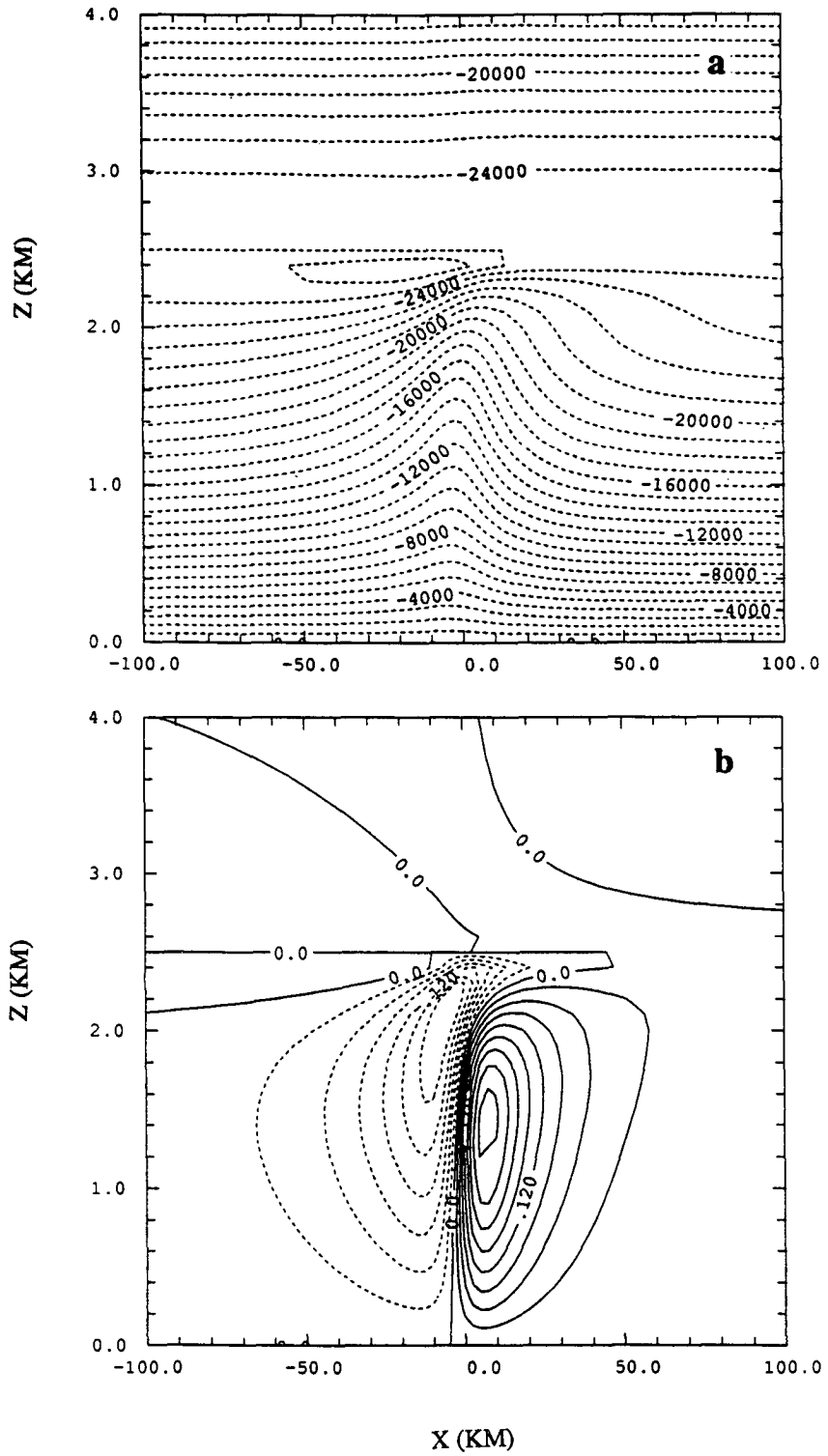

FIG. 3. (a) The total streamfunction calculated by the corresponding dimensional form of Eq. (15) with $N = 0.01\ s^{-1}$, $U_0 = 20\ m\ s^{-1}$, $Q_0 = -1\ J\ kg^{-1}\ s^{-1}$, $d = 2.0$ km, $a_1 = 10$ km, $a_2 = 50$ km, and $H_c = 2.5$ km. The Richardson number associated with the basic flow is 1.56. (b) As in (a), except for the vertical velocity. Contour intervals in (a) and (b) are $1000\ m^2\ s^{-1}$ and $0.03\ m\ s^{-1}$, respectively. Positive (negative) contours are indicated by solid (dashed) lines in the rest of the figures.

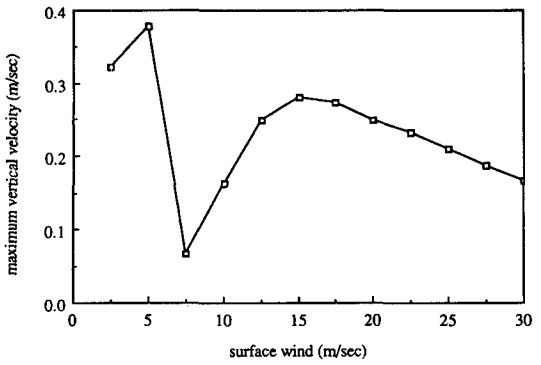

FIG. 4. The domain maximum vertical velocity for different wind shears. The parameters considered are the same as in Fig. 3. The solution is in the dimensional form of Eq. (15).

proximation may appear rather strong near the head of a density current, but the overall balances that determine the density current propagation are hydrostatic (Raymond and Rotunno 1989). In the numerical model, the potential temperature, instead of buoyancy, is predicted. Therefore, Eqs. (2) and (3) are replaced by the following equations:

$$\partial\pi/\partial z = g\theta'/\theta_0, \tag{19}$$

$$D\theta/Dt = \bar{\theta}Q/(c_pT_0) + D_\theta, \tag{20}$$

where $D/Dt = \partial/\partial t + u\partial/\partial x + w\partial/\partial z$. Here θ is the potential temperature, θ' the perturbation potential temperature, and $\bar{\theta}$ the undisturbed mean potential temperature. Notice that in the numerical model, the variables u and θ denote mean plus perturbation quantities.

The governing equations are solved numerically using the finite-difference method. The horizontal derivative terms are approximated by the fourth-order finite-difference scheme, while the vertical derivative terms by the second-order scheme. The leapfrog scheme is used for the time differencing. The finite-difference schemes of the model are similar to the LAMPS model (Perkey 1976). A weak numerical space smoothing based on the fourth-order diffusion is applied to all variables in order to reduce amplitudes of short waves that are not properly represented by the finite-difference approximation and to prevent the nonlinear aliasing. In addition, the Asselin (1972) time filter is used to prevent time splitting due to the leapfrog time differencing. To reduce the reflection of gravity waves from the upper and lateral boundaries, radiation boundary conditions are employed according to the numerical techniques proposed by Klemp and Durran (1983) and Orlanski (1976).

The subgrid-scale mixing processes for momentum (D_u) and potential temperature (D_θ) are parameterized using the first-order closure:

$$D_u = (K_mA)_x + (K_mB)_z, \tag{21a}$$

$$D_\theta = (K_h\theta_x)_x + (K_h\theta_z)_z, \tag{21b}$$

where

$$A = u_x - w_z, \quad B = u_z + w_x,$$

$$K_m = k^2\Delta x\Delta z(A^2 + B^2)^{1/2} \times \max[1 - (K_h/K_m)\mathrm{Ri}, 0]^{1/2},$$

$$\mathrm{Ri} = gd\ln\theta/(A^2 + B^2). \tag{22}$$

Here Δx and Δz are the grid intervals in the horizontal and vertical directions and k is a numerical constant (Lilly 1962). For simplicity, the eddy Prandtl number K_h/K_m is set to one. The diabatic cooling term Q is specified as

$$Q(x, z) = \begin{cases} Q_0, & \text{for } |x - x_0| \leq L \\ & \text{and } 0 \leq z \leq d \\ 0, & \text{for elsewhere,} \end{cases} \tag{23}$$

where Q_0 is the cooling rate, x_0 the cooling center in the horizontal, L the half length of the cooling, and d the cooling depth.

In all simulations except for the case of Fig. 11a, the horizontal and vertical grid intervals are taken to be 2.5 km and 100 m. The time step is 10 s. It is impossible to completely resolve the vertical wavelength in the vicinity of the critical level because it approaches zero there. Even in the nonlinear numerical model, a finer resolution in the vertical is necessary to investigate the wave behavior near the critical level. Varying the vertical grid interval is one way to resolve this problem without requiring large memory and computing time in the model. However, Breeding (1962) showed that the model results with a uniform Δz of 100 m reasonably agree with those with a finer resolution. For all simulations shown in this paper, all parameters are fixed except the surface wind speed. Again, large surface wind means strong wind shear and small Richardson number since the critical height is fixed. The parameters specified are $N = 0.01\ \mathrm{s}^{-1}$, $H_c = 2.5$ km, $Q_0 = -3\ \mathrm{J\ kg^{-1}\ s^{-1}}$, $d = 1.5$ km, and $L = 10$ km. The cooling rate of $Q_0 = -3\ \mathrm{J\ kg^{-1}\ s^{-1}}$ is equivalent to the evaporative cooling produced by a precipitation rate of 7 mm $\mathrm{h^{-1}}$. This value is rather small compared with the cooling rate used in Thorpe et al. (1982). However, since the cooling is applied steadily (more than 2 h) in this study, a relatively small value of the cooling rate appears to be necessary. In addition, this cooling rate is equal to the nondimensional cooling rate of 0.008 in Raymond and Rotunno (1989).

b. Model results and discussion

Figure 5 displays the wind velocity and the potential temperature fields at $t = 7200$ s for a case with $U_0 = 30$

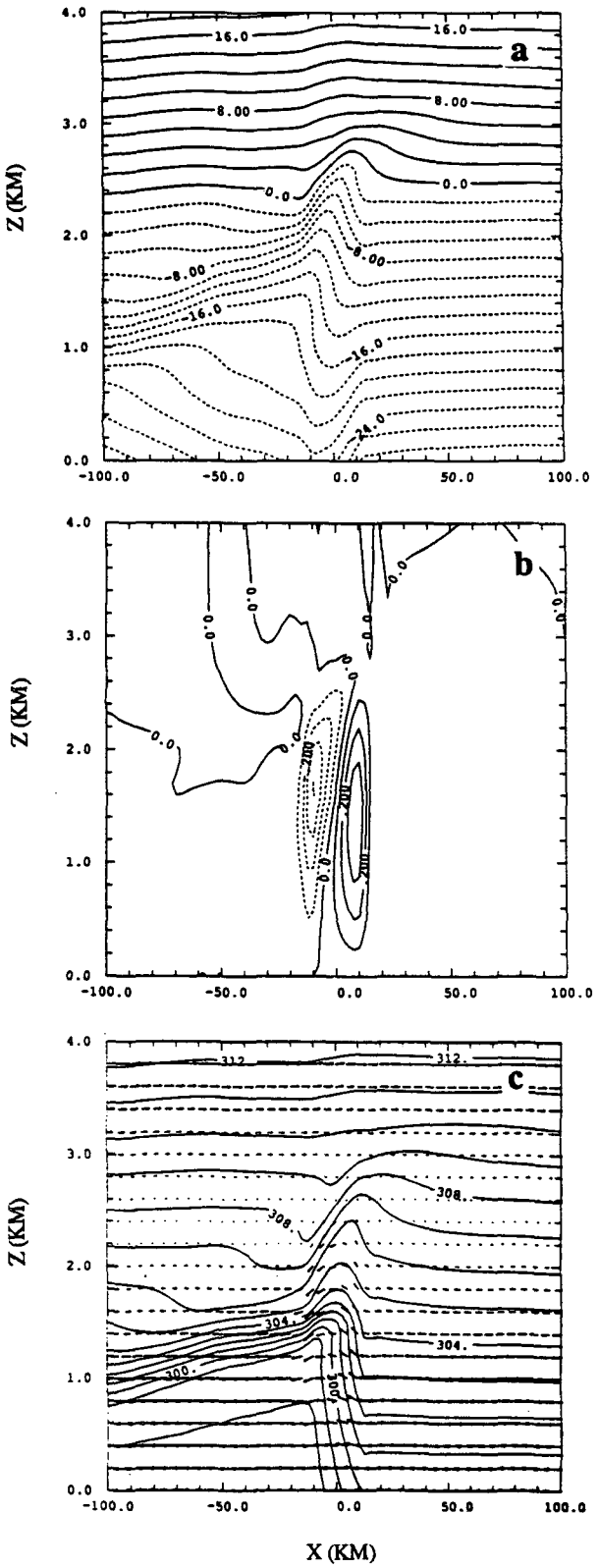

FIG. 5. (a) Horizontal velocity with contour interval of 2.0 m s^{-1}, (b) vertical velocity with contour interval of 0.1 m s^{-1}, and (c) potential temperature (contour interval of 1 K) superimposed on the wind vector field at t = 7200 s when U_0 is 30 m s^{-1}. The Richardson number associated with the basic flow is 0.69. The parameters considered are N = 0.01 s^{-1}, Q_0 = −3 J kg^{-1} s^{-1}, d = 1.5 km, L = 10 km, and H_c = 2.5 km. The vertical velocity in the wind vector is exaggerated by a factor of 30.

m s^{-1}. The flow reaches a steady state rather quickly under this situation. The response in the vicinity of the cooling is similar to the linear steady-state case (Fig. 3) because the nonlinearity parameter, Eq. (10), is about 0.22 in this case. The air parcel decelerates (accelerates) on the upstream (downstream) side of the cooling region. Associated with the horizontal deceleration and acceleration of the air parcel, regions of convergence and divergence, respectively, must exist. The convergence (divergence) then induces an upward (downward) motion on the upstream (downstream) side of the cooling region (Fig. 5b) through the continuity equation. The upward motion on the upstream side of the cooling region is caused by the compensated updraft (Lin and Smith 1986; Lin 1987) and the convergence of the flow there. Unlike the linear solution, the horizontal wind speeds do not approach infinity near the critical layer, where the total horizontal wind speed vanishes, in the nonlinear system.

A region of acceleration exists just below the critical layer and above the cooling region, which is responsible for the downward motion (Fig. 5b). The acceleration in the layer from 1.5 to 2.5 km also helps shift the region of minimum vertical velocity to a higher level than that of the maximum vertical velocity. The wind vector field is shown in Fig. 5c, with the vertical velocity exaggerated by a factor of 30. The horizontal velocity, vertical velocity, and potential temperature fields all indicate that the disturbance is very weak above 3 km, which is caused by the critical layer absorption. This is consistent with the linear theory of Booker and Bretherton (1967), in which they found that gravity waves tend to be attenuated exponentially as they pass through the critical level when the Richardson number is greater than 1/4.

The potential temperature field (Fig. 5c) indicates that a cold pool exists near the surface from the center of the domain to downstream. A weak gust front forms near the center of the domain, associated with the convergence formed by the cold pool and the basic wind advection. Air parcels are lifted up in the vicinity of the gust front and forced downward over the cold pool. The cold pool appears to be stationary and cannot propagate upstream. The strong surface wind tends to retard the upstream propagation of the cold air. The stationarity of the cold pool allows for initiation of convection. Thorpe et al. (1982) used this mechanism for initiating convection in a numerical model. At the upstream edge of the cooling region, the cold pool has a height of about 1.5 km, which is about the height of the specified cooling. The cold pool extends far down-

stream and has a smaller depth because the cold air is swept downstream by the mean wind. It is important to mention that the cold pool acts like a mechanical forcing that forces the air parcel to go upward at the upstream edge. Thus, it may act more or less as a very asymmetric mountain. This behavior is different from the flow over a heat source (e.g., Lin 1987), which allows the air parcel to penetrate the forcing region. The difference results from the fact that the cold air produced by cooling tends to accumulate near the surface while the warm air produced by heating tends to rise. Above the gust front, the cold region extends to the critical layer and tilts upstream or downshear. This region of cold air is formed by the adiabatic cooling associated with the upward-propagating gravity waves rather than by the diabatic cooling. This is evidenced by the upstream tilting of the potential temperature field.

Figure 6 shows the wind velocity and potential temperature fields at $t = 7200$ s for a case similar to that of Fig. 5, except with $U_0 = 20$ m s^{-1}. The Richardson number associated with the basic flow is 1.5. The effective cooling rate is larger in this case because the basic wind speed in the cooling layer is smaller. Under this situation, the cold pool is still unable to propagate upstream. However, the gust front becomes stronger and deeper than the case with $U_0 = 30$ m s^{-1} (Fig. 5). A stronger wave than the previous case is present in the layer of 2 to 3 km. Again, there is no significant wave activity above 3 km. This implies that the waves are absorbed by the critical layer, similar to the previous case. The possibility of wave reflection from the critical level, as suggested by Breeding (1972), will be examined later.

Figure 7 shows the wind velocity and potential temperature fields at $t = 7200$ s for a case similar to that of Fig. 6, except with $U_0 = 10$ m s^{-1}. The Richardson number associated with the basic flow is 6.25. One interesting finding in this case is that the cold pool is able to develop into a density current and propagate upstream. The upstream propagation of the density current in the present case is evidenced by a region of positive horizontal velocity near the surface, which has a maximum value of about 18 m s^{-1} and is located near the head of the density current. The averaged speed of the density current propagation is about 5.6 m s^{-1}. Notice that the propagation speed of the density current increases with time. This is because the strength of the cold pool increases with time due to the steady cooling. Crook and Moncrieff (1988) suggested that the term "density current" can be used only if the surface air on the upstream side of the system does not return to the surface behind the system. Using their definition, both the present case and the flow of Fig. 8 in Raymond and Rotunno (1989) may fall into the category of a gravity wave with stagnation. To avoid ambiguity, we define a *density current* as a propagating

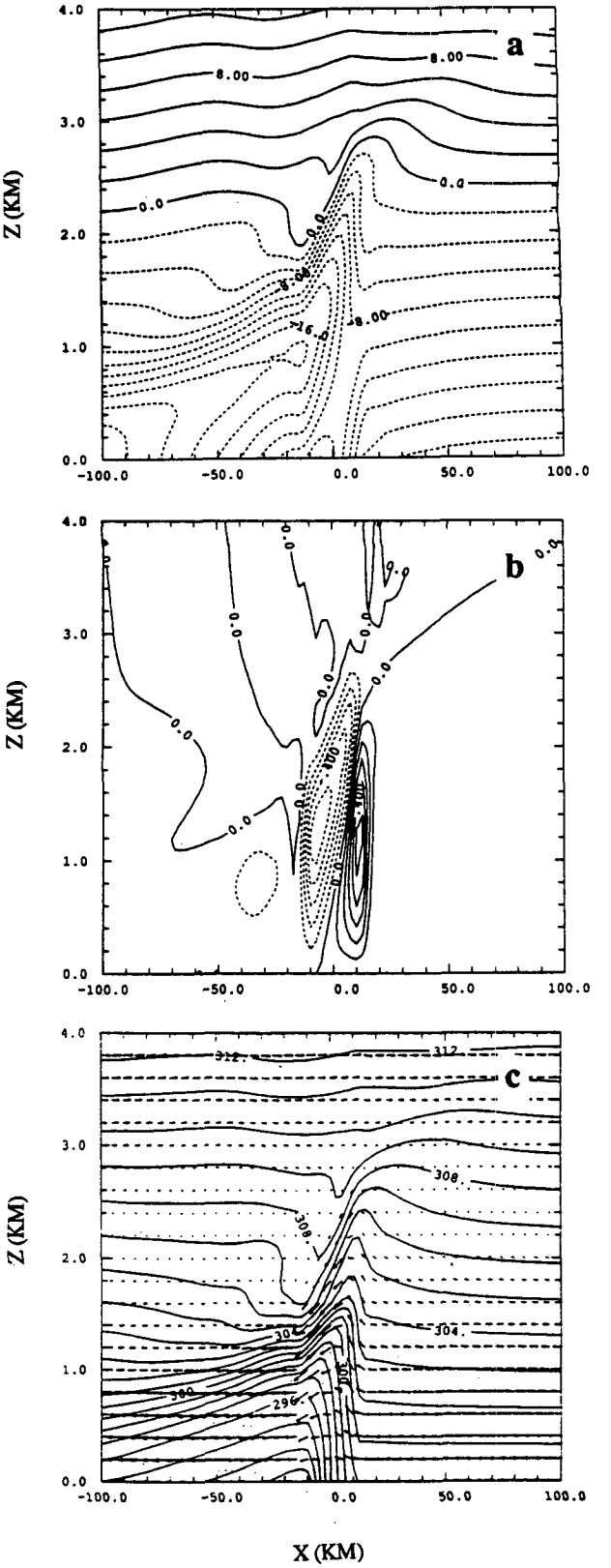

FIG. 6. As in Fig. 5 except with $U_0 = 20$ m s^{-1} and Ri = 1.56.

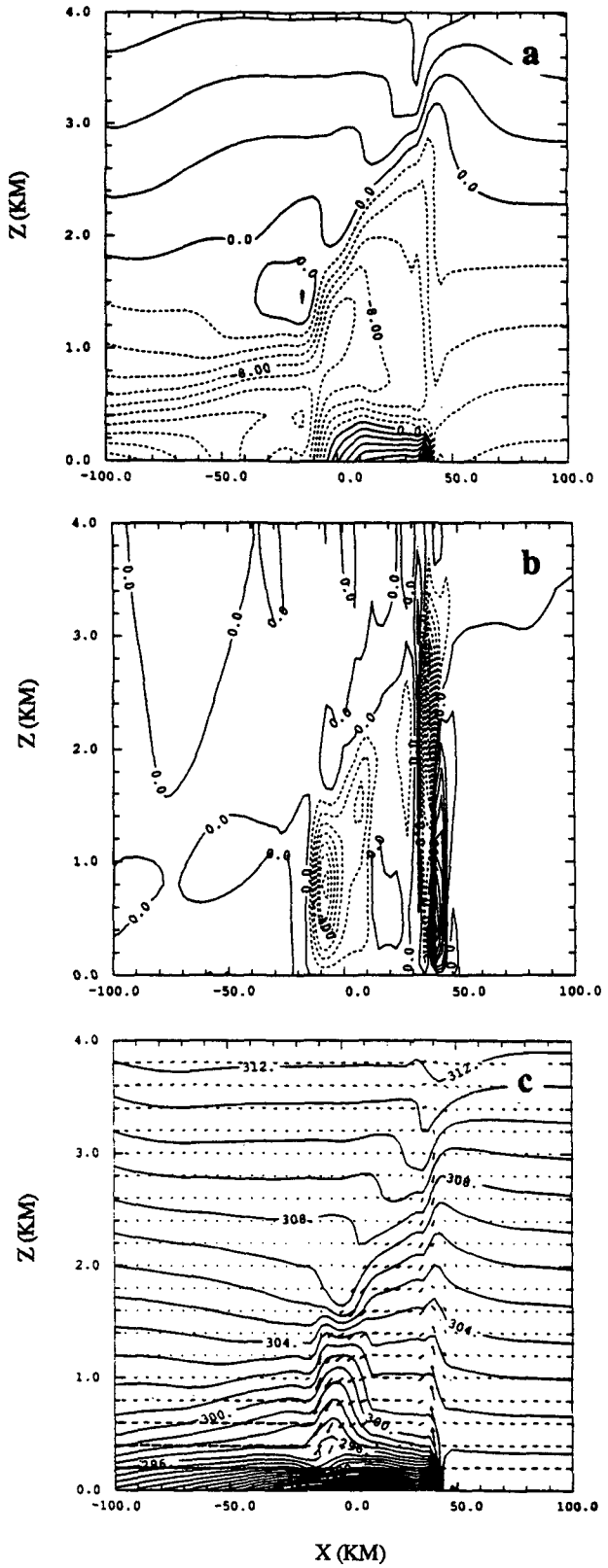

FIG. 7. As in Fig. 5, except with $U_0 = 10$ m s^{-1} and Ri = 6.25.

cold outflow against the ambient fluid in a moving frame with the outflow. The cold pool in previous cases may develop into a density current after 2 h because the steady cooling keeps strengthening the cold pool. In numerical simulations of midlatitude multicellular squall lines, Fovell and Ogura (1989) found that the density current speed is almost linearly proportional to the lower-layer wind shear if the shear is strong. This will predict a zero speed of the density current investigated in this study and other dry-model results (Thorpe et al. 1982; Raymond and Rotunno 1989). For a dry model with specified cooling, such as the present case, the speed of a density current is fixed no matter what value of the inflow speed is used. Because the cooling rate is fixed, the magnitude of the effective cooling that can produce an upstream-propagating outflow decreases as the wind shear increases. Consequently, no upstream propagation of the density current is possible for a strong shear flow. In the real atmosphere with the presence of moisture, the inflow may contribute to either strengthen or weaken the cooling rate and the speed of the density current.

Associated with the region of strong positive horizontal velocity near the surface, a region of strong convergence exists at the head of the density current, near $x = 40$ km. Convergence at the head of a density current has been considered as an important mechanism for the initiation or regeneration of convective storms (Thorpe et al. 1980). A region of strong updraft is produced by this strong convergence zone (Fig. 7b). The maximum vertical velocity reaches about 0.9 m s^{-1}, which is much higher than 0.3 and 0.5 m s^{-1} in the cases of Figs. 5 and 6. Unlike previous cases, this updraft is separated from the downdraft associated with the cooling. The downdraft is located at $x = -10$ km. Above this updraft is a region of strong downdraft associated with the upward-propagating gravity waves. The gravity wave structure can also be found in the potential temperature field (Fig. 7c). The horizontal scale of this gravity wave is about 10 km and is closely related to the scale of the convergence at the head of the density current. The magnitude of the wave increases as it propagates upstream. In the layer from 1.5 to 4 km above the cooling region, a relatively strong disturbance exists that tilts downshear (Figs. 7a,c). It appears that this disturbance is associated with the upward-propagating waves generated by the steady cooling.

The potential temperature field is shown in Fig. 7c. A region of cold air is located in the region below 1.5 km and between $x = 10$ and -10 km. This cold air is produced by the specified cooling. Above this cold pool, a region of warm air exists that extends to 4 km and tilts downshear. This warm air is produced adiabatically by the downdraft associated with the stationary upward-propagating wave. A narrow but deep region of warm air is riding on the density current and propa-

gating upstream with it. This warm air is produced by the strong downdraft (Fig. 7b) above the density current.

From the above results, we may categorize the flow response as a *stationary cold pool case* (Figs. 5 and 6) and the case of Fig. 7 as a *density current case* (Fig. 7) due to their remarkable differences. In order to understand the transient response, we will examine the time evolutions of the vertical velocity for cases of Figs. 6 and 7. Figure 8 shows the vertical-velocity fields at three time steps: namely, 1000, 3000, and 5000 s for both the density current case (Fig. 8a) and the stationary cold pool case (Fig. 8b). During the early stage of the evolution (at 1000 s) for both cases, two regions of upward motion have developed. The stronger one is located upstream; the weaker one, downstream. Both are compensated updrafts associated with the downdraft at the center. The upstream updraft is stronger because it is strengthened by the convergence produced by the inflow. As time proceeds, these two modes propagate out of the cooling region with the cold outflow in opposite directions. The downstream mode propagates faster than the upstream one because it is accelerated up by the advection of the basic wind. Similarly, the downstream mode of the stationary cold pool case (Fig. 8b) propagates faster than that of the density current case (Fig. 8a). In the density current case, the magnitude of the vertical velocity associated with the downstream mode increases as it propagates because the effective cooling increases with time. The upstream mode starts to propagate upstream against the inflow as more cold air is accumulated. Since the cold air outflow is strong enough, the upstream mode splits and propagates away from the cooling region. The magnitude of the vertical velocity for this mode also increases as it propagates because of the steady cooling. The strong convergence at the head of the density current in the lower layer (below 400 m) is responsible for enhancing the updraft there and may regenerate convection ahead of the density current if moisture is abundant enough. This may provide a possible mechanism for long-lived convective systems. This is not true in the stationary cold pool case in which the effective cooling is too weak to push the cold air upstream. The magnitude of the vertical velocity for the upstream mode in this case increases in the beginning and then approaches a steady state. The overall structure of this mode is similar to the linear steady-state solution. Although the stationarity of the updraft may be favorable for generating deep convection, the magnitude of the updraft is only about half that of the density current case.

To investigate the nonlinear effects on the shear flow response to the cooling, we perform one linear modeling simulation for comparison with the nonlinear simulation of Fig. 7. For the linear simulation, one should use parameters different from those used in the nonlinear simulation in order to keep the linear assumption valid. However, a direct comparison between the linear and nonlinear simulations is possible only using the same parameters. Thus, we use the same parameters for the linear simulation (Fig. 9) as in the nonlinear simulation (Fig. 7). For the linear case, the minimum horizontal velocity is located near 1.8 km height at the center of the domain, which is lower than that of the nonlinear case (Fig. 7a). In addition, the minimum value is much larger than that of the nonlinear case. On the other hand, the maximum horizontal velocity near the surface, representing density current, is smaller than that of the nonlinear case. This is due to the advection of the perturbation horizontal velocity, which can produce positive tendency of the horizontal velocity and is ignored in the linear case.

Figure 10 shows the time evolution of the kinetic wave energy for every hour in both linear and nonlinear cases. The kinetic wave energy is defined by $\rho_0(\bar{u}^2 + \bar{w}^2)/2$, where ρ_0 is the ambient density which is assumed to be 1 kg m^{-3} and $\bar{u}$ and $\bar{w}$ are the horizontally averaged velocity perturbations in horizontal and vertical, respectively. The value of kinetic wave energy is maximum at the surface for both cases because the ambient wind is maximum (10 m s^{-1}) there. Above the critical height, the value is almost zero even though the ambient wind is large since the wave cannot penetrate through the critical height from below. The second maximum, near 1.8 km height in the linear case and about 1.2 km in the nonlinear case, appears to be related to the vertical wavelength of the dominant gravity wave. In fact, there are an infinite number of vertical wavelengths $(2\pi U/N)\lambda_z$ between the ground and the critical height in a flow with linear wind shear. If we use the ambient wind speed averaged from the surface to 4 km ($U = 3$ m s^{-1}), the vertical wavelength is about 1.8 km. This is roughly the height of the second maximum in the linear case. Nonlinearity appears to reduce the wave disturbance below the critical level and above the cooling top, while it tends to strengthen the wave disturbance near the surface. In addition, the vertical wavelength of the upward-propagating wave is reduced by the nonlinearity.

To examine the effects of the vertical resolution, we perform a case similar to that in Fig. 7, except with a finer resolution of $\Delta z = 25$ m. The horizontal field is shown in Fig. 11a for comparison. The result is very similar to that of Fig. 7a, except Fig. 7a has a stronger maximum value (18 m s^{-1}) near the surface, compared with that in Fig. 11a (14 m s^{-1}). However, both of them have a minimum value of about -20 m s^{-1}. In addition, the contour line near the top of the model domain is slightly smoother than the case with $\Delta z = 100$ m.

In order to examine the possible artificial wave reflection from the model top, we run a case similar to Fig. 7 except with the model top extended to 8 km.

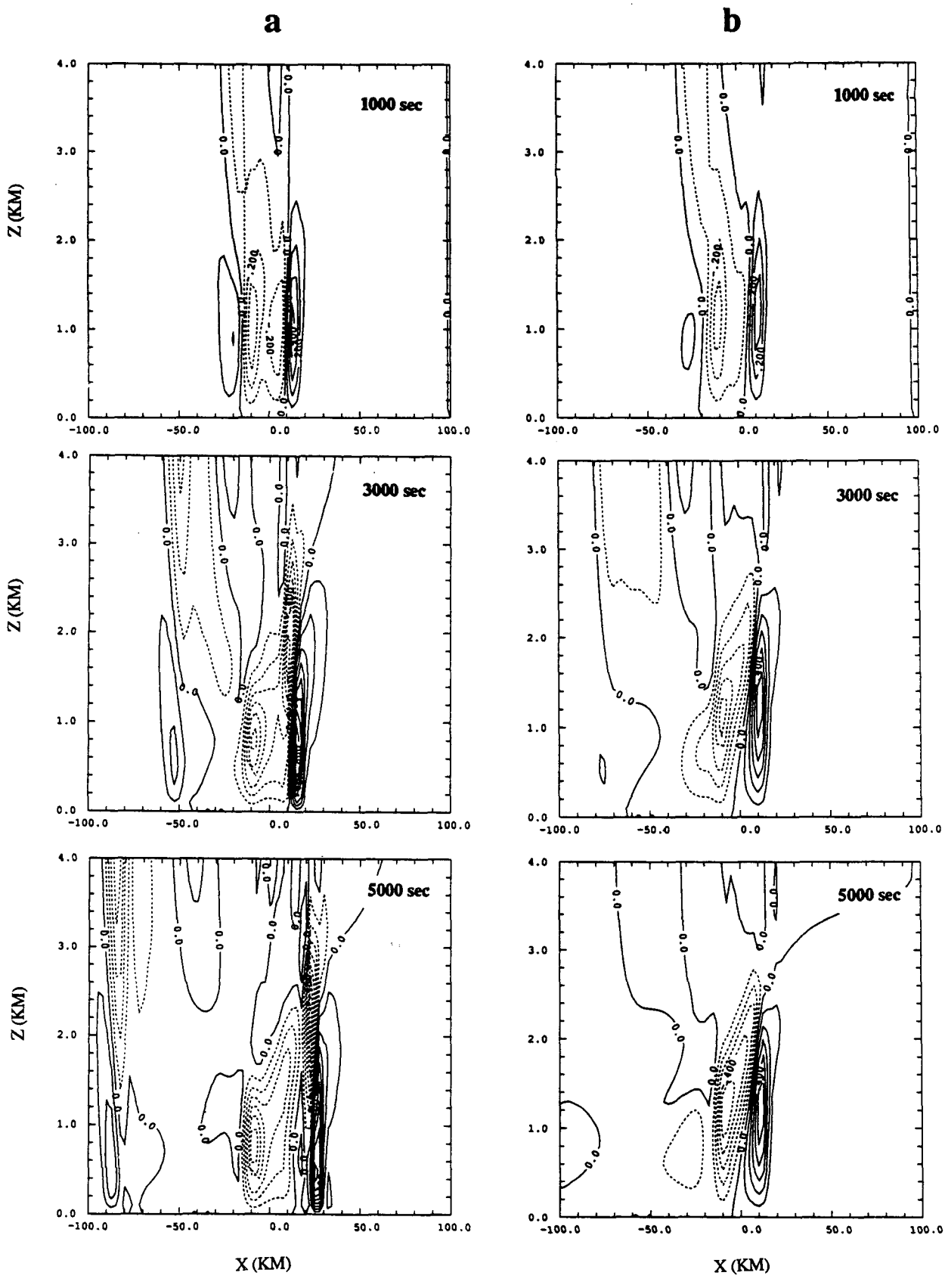

FIG. 8. Sequence of evolving vertical velocity fields corresponding to (a) Fig. 7b and (b) Fig. 6b.

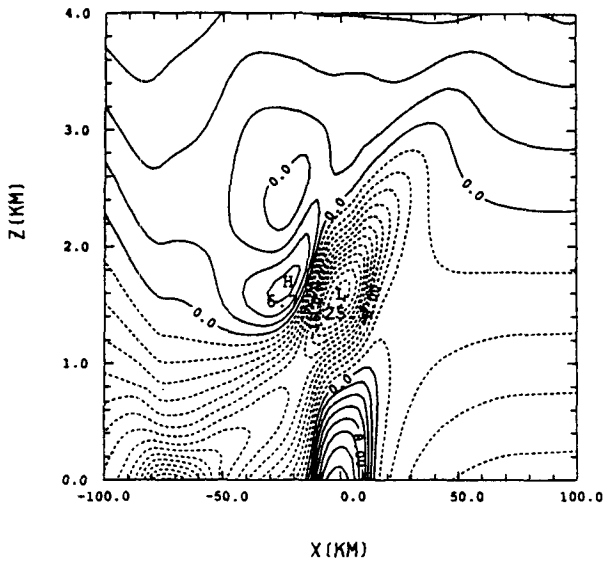

FIG. 9. Horizontal velocity (contour interval of 2 m s^{-1}) at t = 7200 s from the linear numerical simulation with the same parameters used in Fig. 7.

The result is shown in Fig. 11b. Below 4 km, the flow structure is almost identical to Fig. 7a. Above 4 km, there exists very weak wave disturbance since most of the wave energy has been absorbed by the critical level. No obvious wave reflection exists from the model top. This indicates that the upper radiation boundary condition of the numerical model is able to radiate wave energy out.

6. Summary and conclusions

• The response of a two-dimensional stably stratified shear flow with a critical level was studied using both a linear theory and a nonlinear numerical model. The diabatic cooling, which represents the evaporative cooling by falling precipitation, is specified a priori in a fixed region, and the ambient wind is allowed to increase linearly with height and reverse its direction at a certain height. In order to investigate wind shear effects, the magnitude of the surface wind must be varied with other parameters held constant in all simulations.

• From a scale analysis of the governing equations, we found a nonlinear factor, $gQ_0l/(c_pT_0U_0^2N)$, of the thermally induced finite-amplitude waves. Consistent with other linear theories, when the wave approaches the critical level, most of the wave energy is absorbed at the critical level and attenuated exponentially. From a scale analysis of the linear solution, it was shown that the magnitude of the perturbation streamfunction or the vertical velocity is independent of the Richardson number for a given cooling rate and depth. When the thermally induced Froude number (U_0/Nd) is relatively large, the maximum perturbation increases as the Richardson number decreases, while for small Froude number, the maximum perturbation is independent of the Richardson number.

• The linear solutions for different Richardson numbers are characterized by the relative magnitude of three types of speed: basic wind speed, horizontal speed of the gravity wave with a vertical wavelength of $2d$, and upstream propagation speed of the density current. From the scale analysis of the linear system, we found a condition under which the upstream density current is just opposed by the ambient wind. When the shear and the basic wind are of opposite sign in the forcing region, the wind shear can reduce the magnitude of the ratio of the basic wind to the upstream-propagating density current speed. This implies that in the sheared flow, small ambient wind is enough to prevent the upstream propagation of the density current because part of the cooling is used to compensate the positive vorticity associated with the positive vertical wind shear and, consequently, the effective cooling rate or the speed of the density current becomes smaller than that in the uniform wind case.

• In the nonlinear numerical simulations, it was found that the responses of the atmosphere to a steady cooling in a shear flow are categorized as either a *stationary cold pool* or a *density current,* depending upon the strength of the effective cooling or ability of the upstream propagation of the cold outflow. For a strong shear flow, the effective cooling rate becomes weak and the cold pool is stationary with respect to the upstream flow because most of the cooling is used to compensate the positive vorticity associated with the positive wind shear. In this case, the flow quickly reaches a steady state and the response is similar to the linear steady-state case. For a weak shear flow, the cold pool is able to propagate upstream because the effective cooling that increases with time is strong enough to push the outflow against the basic wind. The convergence at the head of the density current in the lower layer is responsible for enhancing the magnitude of the disturbance and controlling the horizontal scale of the updraft there.

• To investigate the nonlinear effects on the shear flow with cooling, both linear and nonlinear numerical model simulations are performed. From the time evolutions of the kinetic wave energy in both linear and nonlinear cases, it is found that the nonlinearity appears to reduce the wave disturbance in the layer below the critical level and above the cooling top, while it tends to strengthen the density current or cold pool near the surface. In addition, the vertical wavelength of the upward-propagating wave is reduced by the nonlinearity.

• In this study, we considered a dry atmosphere only. For the dry model with the specified cooling, the upstream propagation speed of the density current is fixed no matter what value of the basic wind is used. In the

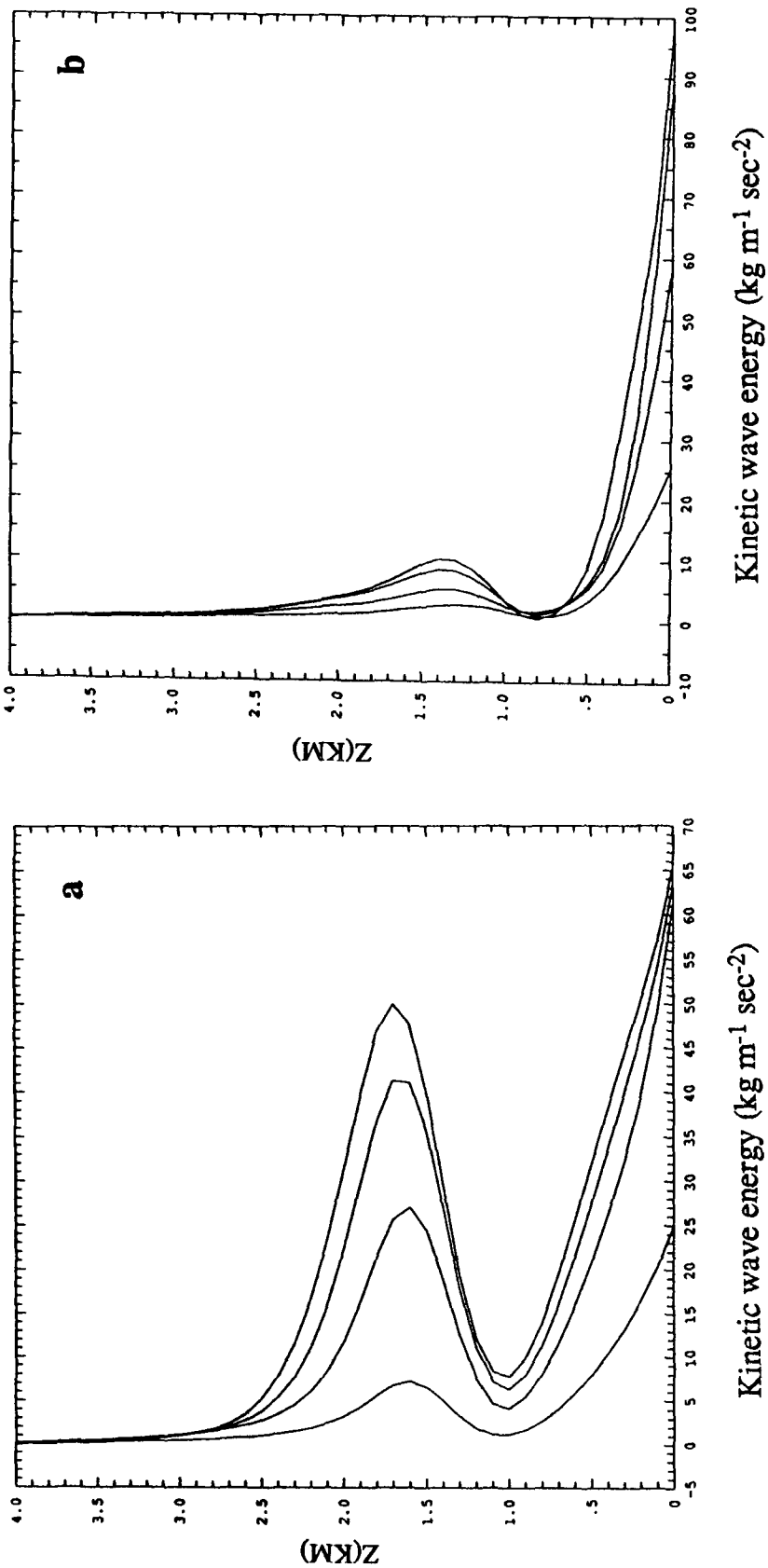

FIG. 10. Time evolutions of the kinetic wave energy for every hour in (a) linear and (b) nonlinear numerical simulations with the same parameters used in Fig. 7.

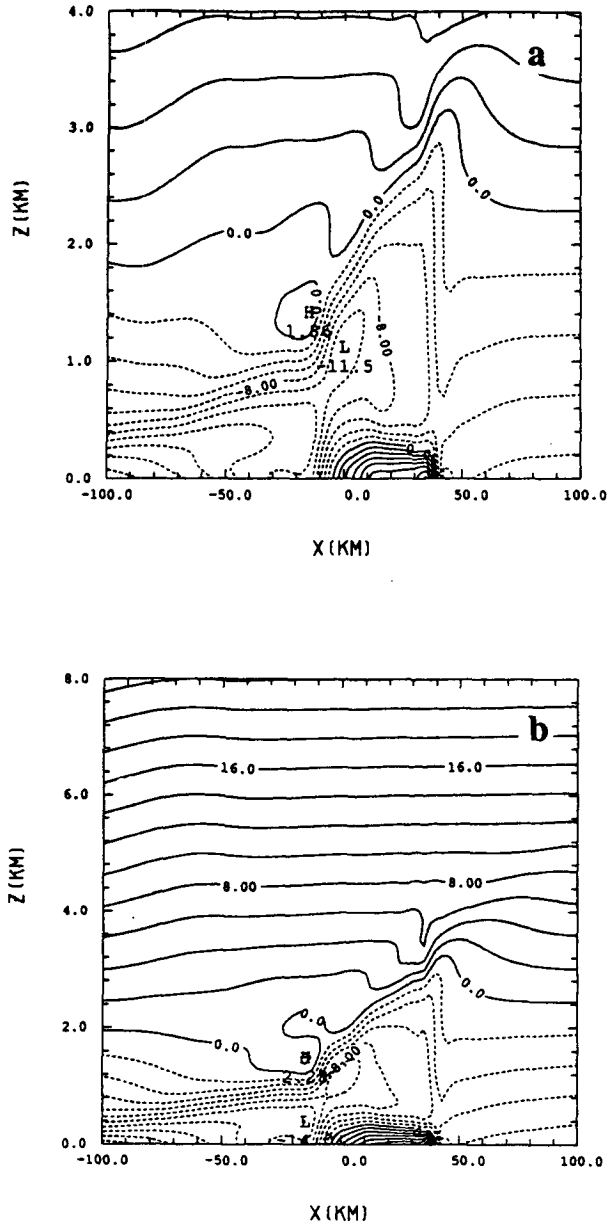

FIG. 11. (a) As in Fig. 7a, except with a finer vertical resolution of Δz = 25 m. (b) Same as in Fig. 7a, except with the model top extended to 8 km.

presence of moisture, the inflow may contribute to either strengthen or weaken the cooling rate and the speed of the density current. These effects are currently under investigation.

Acknowledgments. Discussions with Dr. A. J. Riordan are appreciated. The authors wish to thank Mr. R. P. Weglarz for reading the manuscript. This research was supported by the National Science Foundation under Grants ATM-88-07064 and ATM-88-15780.

REFERENCES

Asselin, R., 1972: Frequency filter for time integrations. *Mon. Wea. Rev.*, **100,** 487–490.

Barcilon, A., and D. Fitzjarrald, 1985: A nonlinear steady model for moist hydrostatic mountain waves. *J. Atmos. Sci.*, **42,** 58–67.

Bluestein, H. B., and M. H. Jain, 1985: Formation of mesoscale lines of precipitation: Severe squall lines in Oklahoma during spring. *J. Atmos. Sci.*, **42,** 1711–1732.

Booker, J. R., and F. P. Bretherton, 1967: The critical layer for internal gravity waves in a shear flow. *J. Fluid Mech.*, **27,** 513–539.

Breeding, R. J., 1971: A non-linear investigation of critical levels for internal atmospheric gravity waves. *J. Fluid Mech.*, **50,** 545–563.

Bretherton, C., 1988: Group velocity and the linear response of stratified fluids to internal heat or mass sources. *J. Atmos. Sci.*, **45,** 81–93.

Charba, J., 1974: Application of gravity current model to analysis of a squall-line gust front. *Mon. Wea. Rev.*, **102,** 140–156.

Clark, T. L., and W. R. Peltier, 1977: On the evolution and stability of finite amplitude mountain waves. *J. Atmos. Sci.*, **34,** 1715–1730.

Crook, N. A., and M. W. Moncrieff, 1987: The effect of large-scale convergence on the generation and maintenance of deep moist convection. *J. Atmos. Sci.*, **45,** 3606–3624.

Droegemeier, K. K., and R. B. Wilhelmson, 1985a: Three-dimensional numerical modeling of covection produced by interacting thunderstorm outflows. Part I: Control simulation and low-level moisture variations. *J. Atmos. Sci.*, **42,** 2381–2403.

——, and ——, 1985b: Three-dimensional numerical modeling of covection produced by interacting thunderstorm outflows. Part II: Variations in vertical wind shear. *J. Atmos. Sci.*, **42,** 2404–2414.

Eliassen, A., and E. Palm, 1960: On the transfer of energy in stationary mountain waves. *Geofys. Publ.*, **22,** 1–23.

Fovell, R. G., and Y. Ogura, 1989: Effect of vertical wind shear on numerically simulated multicell storm structure. *J. Atmos. Sci.*, **46,** 3144–3176.

Klemp, J. B., and D. K. Lilly, 1978: Numerical simulation of hydrostatic mountain waves. *J. Atmos. Sci.*, **35,** 78–108.

——, and D. R. Durran, 1983: An upper boundary condition permitting internal gravity wave reflection in numerical mesoscale models. *Mon. Wea. Rev.*, **111,** 430–444.

Lilly, D. K., 1962: On the numerical simulation of buoyant convection. *Tellus*, **14,** 148–172.

Lin, Y.-L., 1987: Two-dimensional response of stably stratified shear flow to diabatic heating. *J. Atmos. Sci.*, **44,** 1375–1393.

——, and R. B. Smith, 1986: Transient dynamics of airflow near a local heat source. *J. Atmos. Sci.*, **43,** 40–49.

——, and Shiaolin Li, 1988: Three-dimensional response of a shear flow to elevated heating. *J. Atmos. Sci.*, **45,** 2987–3002.

Matthews, D. A., 1981: Observations of cloud arc triggered by thunderstorm outflow. *Mon. Wea. Rev.*, **109,** 2140–2157.

Mitchell, K. E., and J. B. Hovermale, 1977: A numerical investigation of the severe thunderstorm gust front. *Mon. Wea. Rev.*, **105,** 657–675.

Newton, C. W., 1950: Structure and mechanism of the prefrontal squall line. *J. Meteor.*, **7,** 210–222.

——, and H. R. Newton, 1959: Dynamical interaction between large convective clouds and environment with vertical shear. *J. Meteor.*, **16,** 483–496.

Ogura, Y., and M.-T. Liou, 1980: The structure of a midlatitude squall line: A case study. *J. Atmos. Sci.*, **37,** 553–567.

Orlanski, I., 1976: A simple boundary condition for unbounded hyperbolic flows. *J. Comput. Phys.*, **21,** 251–269.

Pastushkov, R. S., 1975: The effects of vertical wind shear on the evolution of convective clouds. *Quart. J. Roy. Meteor. Soc.*, **101,** 281–291.

Peltier, W. R., and T. L. Clark, 1979: The evolution and stability of

finite-amplitude mountain waves. Part II: Surface wave drag and severe downslope windstorms. *J. Atmos. Sci.*, **36,** 1498–1529.

Perkey, D. J., 1976: A description and preliminary results from a fine-mesh model for forecasting quantitative precipitation. *Mon. Wea. Rev.*, **104,** 1513–1526.

Raymond, D. J., 1984: A wave-CISK model of squall lines. *J. Atmos. Sci.*, **41,** 1946–1958.

——, 1986: Prescribed heating of a stratified atmosphere as a model for moist convection. *J. Atmos. Sci.*, **43,** 1101–1111.

——, and R. Rotunno, 1989: Response of a stably stratified flow to cooling. *J. Atmos. Sci.*, **46,** 2830–2837.

Rotunno, R., J. B. Klemp and M. L. Weisman, 1988: A theory for strong, long-lived squall lines. *J. Atmos. Sci.*, **45,** 463–485.

Seitter, K. L., 1986: A numerical study of atmospheric density current motion including the effects of condensation. *J. Atmos. Sci.*, **43,** 3068–3076.

Smith, R.B., and Y.-L. Lin, 1982: The addition of heat to a stratified airstream with application to the dynamics of orographic rain. *Quart. J. Roy. Meteor. Soc.*, **108,** 353–378.

Thorpe, A. J., M. J. Miller and M. W. Moncrieff, 1980: Dynamical models of two-dimensional downdraughts. *Quart. J. Roy. Meteor. Soc.*, **106,** 463–484.

——, ——, and ——, 1982: Two-dimensional convection in non-constant shear: A model of mid-latitude squall lines. *Quart. J. Roy. Meteor. Soc.*, **108,** 739–762.

Weisman, M. L., and J. B. Klemp, 1982: The dependence of numerically simulated convective storms on vertical wind shear and buoyancy. *Mon. Wea. Rev.*, **110,** 504–520.